Journal of Materials Chemistry B

ROYAL SOCIETY OF CHEMISTRY

PAPER

View Article Online
View Journal | View Issue

Cite this: J. Mater. Chem. B, 2022, 10, 6808

An organic transistor for the selective detection of tropane alkaloids utilizing a molecularly imprinted polymer†

Qi Zhou, [a] Yui Sasaki, [a] Kohei Ohshiro, [a] Haonan Fan, [a] Valentina Montagna, [b] Carlo Gonzato, [b] Karsten Haupt *[b] and Tsuyoshi Minami *[a]

Received 19th May 2022,
Accepted 28th June 2022

DOI: 10.1039/d2tb01067d

rsc.li/materials-b

This study proposes a chemical sensing approach for the selective detection of tropane alkaloid drugs based on an extended-gate-type organic field-effect transistor (OFET) functionalized with a molecularly imprinted polymer (MIP). From the viewpoint of pharmaceutical chemistry, the development of versatile chemical sensors to determine the enantiomeric purity of over-the-counter (OTC) tropane drugs is important because of their side effects and different pharmacological activities depending on their chirality. To this end, we newly designed an OFET sensor with an MIP (MIP-OFET) as the recognition element for tropane drugs based on a high complementarity among a template (*i.e.*, (*S*)-hyoscyamine) and functional monomers such as *N*-isopropylacrylamide and 2,2-dimethyl-4-pentenoic acid. Indeed, the MIP optimized by density functional theory (DFT) has succeeded in the sensitive and selective detection of (*S*)-hyoscyamine (as low as 1 μM) by the combination of the OFET with highly selective recognition sites in the MIP. The MIP-OFET was further applied to determine the enantiomeric excess (ee) of commercially available (*S*)-hyoscyamine, and the linearity changes in the threshold voltages of the OFET corresponded to the % ee values of (*S*)-hyoscyamine. Overall, the validation with tropane alkaloids revealed the potential of the MIP combined with OFET as a chemical sensor chip for OTC drugs in real-world scenarios.

1. Introduction

Alkaloid drugs classified in natural products,[1] such as narcotics and psychotropics, possess strong pharmacological activity toward the nervous system because positively charged nitrogen atoms in these drugs are capable of binding to protein receptors through electrostatic interactions.[2] Among them, tropane skeletons based on 8-azabicyclo[3.2.1]octane are employed as the main component of drugs including atropine, scopolamine, *etc.*,[3] while such muscarinic blocking drugs could potentially evoke side effects (hallucination, memory impairment, blurred vision, *etc.*).[4] In particular, atropine is one of the antidotes to treat intoxications by organophosphorus derivatives, whereas relationships between these neurobiological side effects and the tropane drugs are still unclear.[5] In addition, the pharmacological activity of tropane drugs significantly depends on their chirality. Indeed, atropine is racemic hyoscyamine, and only the (*S*)-hyoscyamine enantiomer shows pharmacological activity.[4] Taking into consideration the strict regulations concerning enantiomeric purity in the pharmaceutical industry, the accurate and easy determination of enantiomeric excess (ee) of over-the-counter (OTC) drugs is required.[6–9]

To date, the detection of atropine has been performed by utilizing liquid chromatography equipped with tandem mass spectrometry, which achieved the % ee determination of atropine.[10,11] However, such conventional instrumental methods are complicated and time-consuming because of the preprocessing of samples. Therefore, we focused on an organic field-effect transistor (OFET) device[12–18] as a sensing platform for tropane alkaloid detection. The transistor characteristics rely on potential changes on a gate electrode.[19] Indeed, OFETs can quantify chemical information by an appropriate sensor design utilizing the gate electrode. In an extended-gate-type OFET, a molecular recognition scaffold on the separated gate

[a] *Institute of Industrial Science, The University of Tokyo, 4-6-1 Komaba, Meguro-ku, Tokyo, 153-8505, Japan. E-mail: tminami@iis.u-tokyo.ac.jp*
[b] *CNRS Enzyme and Cell Engineering Laboratory, Université de Technologie de Compiègne, Rue du Docteur Schweitzer, CS 60319, 60203 Compiègne Cedex, France. E-mail: karsten.haupt@utc.fr*

† Electronic supplementary information (ESI) available: Characterization of the MIP and the extended-gate electrode, FT-IR, FE-SEM, FM-AFM, DPV, DFT calculation results, fabrication details and basic characteristics of the OFET, selectivity test, and HPLC charts of enantiomeric excess of (*S*)-hyoscyamine. See DOI: https://doi.org/10.1039/d2tb01067d

electrode (*i.e.*, extended-gate) as the sensing part is connected to the gate of the OFET, which allows chemical sensing in aqueous media.[20–22]

For the detection of tropane derivatives, elaborate receptor designs considering high steric hindrance are necessary.[23] Conventional alkaloid sensors based on cavity molecules and molecular clefts have been widely studied,[23–28] but the development of easy-to-use drug sensors is still challenging because of the difficulty of appropriate receptor designs. In this regard, molecular imprinting is capable of generating cavities for specific analyte recognitions by noncovalent interactions (hydrogen bonds, π–π interactions, electrostatic interactions, *etc.*) in synthetic polymers (molecularly imprinted polymers, MIPs), achieving highly sensitive and selective detection.[29–35] With this three-dimensional recognition space, MIPs were shown to successfully detect tropane drugs.[36–38] However, previous works on the use of MIPs for the detection of atropine did not report on the selective discrimination of (*S*)-hyoscyamine.[39–42] Besides, previous reports have confirmed that MIPs can be formed as thin layers or membranes on substrates including electrodes,[43–46] interfacing MIPs with the extended-gate electrode should be possible. Indeed, the detectability of extended-gate-type inorganic FETs functionalized with MIPs for various chemical species has already been reported.[47–49] Hence, we propose herein an extended-gate-type OFET functionalized with a novel MIP (MIP-OFET) based on poly(*N*-isopropylacrylamide-*co*-2,2-dimethyl-4-pentenoic acid-*co*-*N*,*N*′-methylenebisacrylamide) (*p*(NIPAM-*co*-DMPA-*co*-MBAAM)) for the detection of (*S*)-hyoscyamine and its ee determination (Fig. 1).

2. Experimental

2.1. Materials

Reagents and solvents employed in this study were commercially available and used as supplied. *N*-Isopropylacrylamide (NIPAM),[50] 2,2-dimethyl-4-pentenoic acid (DMPA), *N*,*N*′-methylenebisacrylamide (MBAAM),[43] and ammonium persulfate for the synthesis of an MIP and a non-imprinted polymer (NIP), tetradecylphosphonic acid for the dielectric layer, and the analytes such as (*S*)-hyoscyamine, atropine, tropine, solifenacin succinate, tropicamide, and oxybutynin hydrochloride were purchased from Tokyo Chemical Industry Co., Ltd. The reagents purchased from FUJIFILM Wako Pure Chemical Industries, Ltd were potassium chloride (KCl), hydrogen tetrachloroaurate(III) tetrahydrate ($HAuCl_4$), *N*-ethylethanamine and tetramethylethylenediamine (TEMED). Poly{2,5-bis(3-tetradecylthiophen-2-yl)thieno[3,2-*b*]thiophene} (PBTTT-C_{14}),[51] tropic acid, and 1,2-dichlorobenzene were purchased from Merck KGaA. The organic solvents and reagents obtained from Kanto Chemical Co., Inc. were 2-propanol, potassium hexacyanoferrate(III) ($K_3Fe(CN)_6$), sodium hydroxide, *n*-hexane, and disodium hydrogenphosphate dodecahydrate ($Na_2H_2PO_4$). For the device fabrication, a glass substrate (model Eagle XG, 2 cm × 2.5 cm), gold (Au) particles, and aluminum (Al) wire (1ϕ) were purchased from Corning, Inc., Tanaka Kikinzoku Kogyo Co., Ltd, and Furuuchi Chemical Co., Ltd, respectively. A silver paste (Dotite, type: D-500) purchased from Fujikura Kasei Co., Ltd was utilized for the OFET measurements. The electrochemical measurements were carried out using a Pt wire counter electrode and an Ag/AgCl reference electrode (model: RE-1B), which were purchased from BAS Inc. CYTOP™ (model CTL-809M) with perfluorotributylamine and polyethylene naphthalate (PEN) were supplied by AGC Co., Ltd and TOYOBO Co., Ltd, respectively. Aqueous solutions for all experiments were prepared by using Milli-Q water (18.2 MΩ cm). The enantiomeric purity of hyoscyamine was investigated by high-performance liquid chromatography (HPLC) with a chiral column (Daicel CHIRALCEL OZ-H). The enantiomeric purity of the commercially available (*S*)-hyoscyamine was determined to be 90.2% ee (Fig. S16, ESI†).

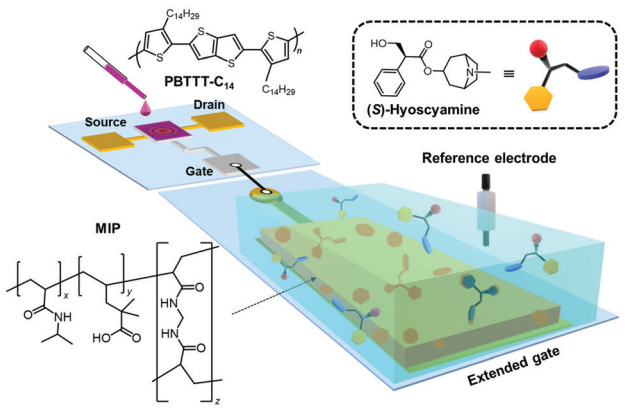

Fig. 1 Schematic illustration of the tropane drug sensor based on the extended-gate type OFET functionalized with the MIP.

2.2. Measurements

The complex of monomers with (*S*)-hyoscyamine was optimized by density functional theory (DFT) calculations using a package of Gaussian 16 REV. C. 011.[52] Chronoamperometry and differential pulse voltammetry (DPV) were carried out on an SP-300 potentiostat (Biologic). In the electrochemical measurements, the potential was scanned from 0 V to 0.45 V in $K_3Fe(CN)_6$ (5 mM) with phosphate buffer (100 mM, pH 7.0) containing KCl (100 mM) at 25 °C. The synthesized MIP was evaluated by Fourier transform infrared spectrophotometry (FT-IR) (a NicoletiS5, Thermo Fisher Scientific Inc.) with a KBr pellet or with a variable angle grazing angle ATR (Harrick Scientific), field-emission scanning electron microscopy (FE-SEM) (a JSM6330F, JEOL), and frequency modulation atomic force microscopy (FM-AFM) (a NanoWizard® 3 BioScience AFM, Bruker). The electrical characteristics of all OFET devices were measured using a source meter (Keithley 2602B).

2.3. Fabrication of the MIP and NIP electrodes

NIPAM (83 mg, 0.73 mmol), MBAAM (3 mg, 0.02 mmol), (*S*)-hyoscyamine (53 mg, 0.18 mmol), and DMPA (25 μL, 0.18 mmol) were dissolved in Milli-Q water (2.5 mL), and then the mixture was stirred for 20 min at 25 °C under an inert atmosphere. After becoming a colorless and transparent solution, TEMED (2.7 μL,

0.018 mmol) was added to the mixture solution and stirred for 2 min. Then, ammonium persulfate (3 mg, 0.01 mmol) was added to the mixture solution, followed by stirring for 2 min. After maintaining the aqueous solution for 8 h at 25 °C under an inert atmosphere, a colorless macro hydrogel was obtained. The hydrogel was washed with a HCl solution (10 mM) 3 times. For the characterization of the obtained polymer by FT-IR, the hydrogel was dried at 70 °C for 5 h by using a vacuum drying oven (AVO-200NB, ETTAS). The NIP was synthesized according to the above-mentioned procedure without using (*S*)-hyoscyamine, while NaOH (2 mg, 0.05 mmol) was added to improve the solubility of DMPA.

The extended-gate Au electrode with 15 mm^2 of conductive area and 100 nm thickness was fabricated on the PEN film by utilizing thermal evaporation equipment (SVC-700TMSG/SVC-7PS80, SANYU Electron). A Au nanostructure (AuNS) was modified on the surface of the extended-gate electrode in a $HAuCl_4$ solution (100 mM) by chronoamperometry based on a three-electrode system. The potential was fixed at −0.1 V for 60 s. The treated electrode was rinsed with ultrapure water 3 times, followed by drying with a N_2 gas flow. The MIP layer was synthesized by drop-casting the aqueous solution containing monomers, (*S*)-hyoscyamine, and the initiator (*i.e.*, the combination of TEMED and ammonium persulfate) (8 μL) onto the extended-gate electrode. The treated electrode was kept at 25 °C for 8 h under ambient conditions to attach the MIP to the surface of the AuNS on the extended-gate electrode. The electrode was rinsed with the HCl solution (10 mM) 3 times and subsequently immersed in the phosphate buffer (100 mM, pH 7.0) containing KCl (100 mM) at 25 °C for 4 h for removing the residue of the template. The NIP-attached electrode was fabricated according to the above-mentioned procedure without (*S*)-hyoscyamine. The MIP or NIP-attached electrode for FE-SEM and FT-IR characterization was dried at 70 °C for 5 h in a vacuum drying oven.

2.4. Fabrication and operation of the extended-gate-type OFET

Vacuum thermal evaporation equipment was applied to fabricate an aluminium gate electrode (30 nm in thickness) on a glass substrate. The aluminium oxide formed by a reactive ion etching method (SAMCO RIE-10NR) was treated with tetradecylphosphonic acid to form a double dielectric layer. Next, source and drain Au electrodes (30 nm in thickness) were deposited using vacuum thermal evaporation equipment. Subsequently, a 1,2-dichlorobenzene solution containing PBTTT-C_{14} was drop cast onto a channel region of the OFET. Finally, the surface of the polymer semiconductive layer was fully covered with CYTOP™. The MIP- or NIP-modified extended-gate electrode was connected to the OFET through a copper conductive cable and the gate voltage was applied through the Ag/AgCl reference electrode. The detectability of the extended-gate-type OFET was assessed under ambient conditions. The fabricated OFET device showed low-voltage operable transistor characteristics ($<|3|$ V), which was suitable for chemical sensing applications. More details of the fabrication process and basic transistor characteristics are summarized in the ESI.†

3. Results and discussion

3.1. Optimization and characterization of the MIP and its modification on the extended-gate electrode

NIPAM and DMPA were selected as the main monomers, because these monomers possess amide and carboxy groups capable of forming hydrogen bonds with the target (*S*)-hyoscyamine. Moreover, DMPA was selected owing to the steric effect derived from its branch methyl groups for the detection of the bulky structural drug.[53] Besides, MBAAM was employed as the crosslinker,[54] resulting in a 3D MIP network for increasing the specific surface area (*vide infra*). To design the MIP for (*S*)-hyoscyamine, DFT calculation was performed by Gaussian 16 at the B3LYP(D3BJ)/def2SVP level with the IEFPCM solvent model (solvent set as water),[55–58] the result of which was visualized by GaussView 6.0.16.[59] Four types of complexes composed of NIPAM, DMPA, and (*S*)-hyoscyamine at different molar ratios were optimized by DFT calculation. In this regard, the binding energies were precisely calculated with the IEFPCM solvent model and the counterpoise method, which could decrease the influence of the basis set superposition error (BSSE) (Table S1, ESI†). Among them, the complex with the molar ratio (NIPAM: DMPA: (*S*)-hyoscyamine = 4 : 1 : 1) showed the lowest binding energy (−107.74 kJ mol^{-1}), which revealed the high complementarity through six hydrogen bonds among (*S*)-hyoscyamine, NIPAM, and DMPA (Fig. 2). Therefore, the MIP was synthesized by radical polymerization according to the above molar ratio. The DPV measurements of the MIP were carried out to evaluate the changes in the peak current after the template extraction. Almost no changes in the peak current after third-time extraction implied the removal of the template completely (Fig. S5, ESI†). The obtained product was characterized by FT-IR and the absorption peaks corresponding to C=O stretching (1727 cm^{-1} for carboxylic acid, 1646 cm^{-1} for

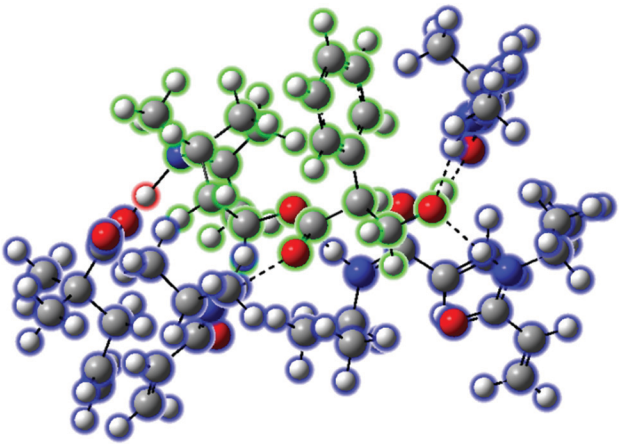

Fig. 2 The molecular complex (NIPAM : DMPA : (*S*)-hyoscyamine = 4 : 1 : 1) optimized by DFT calculation at the B3LYP (D3BJ)/def2SVP level with the IEFPCM solvent model (solvent set as water).

amide), N–H stretching (3305 cm^{-1}), C–C stretching of C–CO–O (1166 cm^{-1}), C–N stretching (1369 cm^{-1}), C–H stretching (2969 cm^{-1}), N–H bending (1540 cm^{-1}) and CH_2 bending (1454 cm^{-1}) bands supported the successful preparation of the MIP [*i.e.*, *p*(NIPAM-*co*-DMPA-*co*-MBAAM)] (Fig. S1(A), ESI†). Meanwhile, the FT-IR result of the NIP showed similar peaks (Fig. S1(B), ESI†), as expected due to the equivalent monomer composition of NIP and MIP.

Next, chronoamperometry was utilized to form the AuNS layer[60] on the thermally deposited Au extended-gate electrode, which could enhance the adhesion by physisorption between the MIP layer and the Au electrode. The surface morphology of the polymer-attached extended-gate electrodes was evaluated by FE-SEM and FM-AFM. The FE-SEM image of the MIP indicated that a porous xerogel was formed with some macropores, offering a large specific surface area. In addition, sharp architectures derived from gold needles were observed (Fig. S3(A), ESI†). Meanwhile, the NIP showed a rather plain surface with fewer macropores (Fig. S3(B), ESI†). Moreover, the FM-AFM image of the bare Au electrode showed low surface roughness with a root mean square deviation (R_q) of ~5 nm (Fig. S4(A), ESI†), while the AuNS-modified Au electrode displayed higher surface roughness with R_q of ~220 nm (Fig. S4(B), ESI†). Furthermore, a decrease in the surface roughness was observed in the MIP-AuNS-modified electrode (R_q: ~144 nm) (Fig. 3). The observed change in the R_q value after immobilization of the MIP suggested that the surface of the AuNS layer was fully covered by the MIP layer with ~200 nm thickness. On the other hand, the NIP (*i.e.*, the chemically identical reference polymer synthesized without the template) showed a rather plain surface (R_q: ~120 nm) with fewer macropores (Fig. S4(C), ESI†) as also observed in the FE-SEM. Such a difference in the surface morphology was probably derived from the extraction of the template that represented as much as ~16 mol% of all components. The FT-IR (ATR) spectrum of the electrode further supported the attachment of the MIP on the electrode by the observed absorption peaks originating from *p*(NIPAM-*co*-DMPA-*co*-MBAAM) (Fig. S2, ESI†).

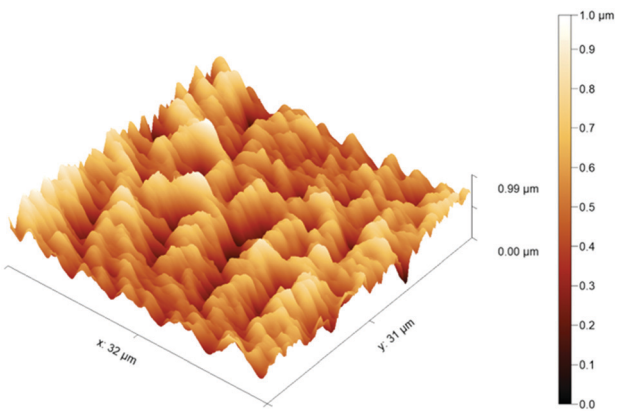

Fig. 3 The FM-AFM image of the MIP-gold nanostructure (AuNS)-attached extended-gate electrode.

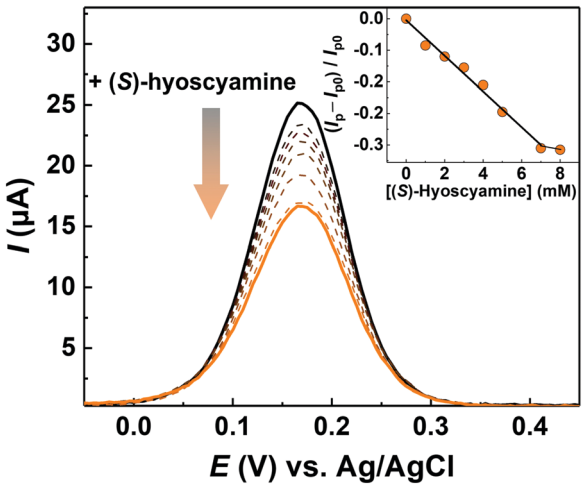

Fig. 4 DPV results of the MIP-AuNS electrode by adding (*S*)-hyoscyamine in a phosphate buffer (100 mM, pH 7.0) containing $K_3Fe(CN)_6$ (5 mM) and KCl (100 mM) at 25 °C. Inset represents the ratio of the peak current (I_p) changes of the MIP-AuNS electrode upon adding (*S*)-hyoscyamine. The terms I_{p0} and I_p indicate the peak currents before and after adding (*S*)-hyoscyamine, respectively. [(*S*)-hyoscyamine] = 0.0–8.0 mM.

Subsequently, the detectability of the MIP-AuNS-attached electrode for (*S*)-hyoscyamine was investigated by DPV (Fig. 4). Here, the MIP-AuNS-attached electrode, the Ag/AgCl electrode, and the Pt wire played roles as the working electrode, the reference electrode, and the counter electrode, respectively. As a negative control experiment, the AuNS-extended-gate electrode functionalized with the NIP (NIP-AuNS electrode) that did not contain (*S*)-hyoscyamine during polymerization was also assessed. The peak current (I_p) of the MIP-AuNS-modified Au electrode decreased with an increase of (*S*)-hyoscyamine concentration, indicating that the adsorption of (*S*)-hyoscyamine prevented the electrochemical redox reaction of the ferricyanide anion.[61] On the other hand, the peak current of the NIP-AuNS electrode showed a weaker response compared with that of the MIP-AuNS electrode, implying that the specific binding sites in the MIP-AuNS electrode contributed to the response of (*S*)-hyoscyamine (Fig. S6, ESI†).

3.2. Detection of (*S*)-hyoscyamine by the extended-gate-type OFET

The electrical detection of (*S*)-hyoscyamine by using the MIP-OFET was performed in a phosphate buffer (100 mM, pH 7.0 at 25 °C) containing KCl (100 mM). Under these conditions, almost all amino groups of the target are protonated, while almost all carboxy groups of the MIP are deprotonated.[62] Hence, strong electrostatic interactions and hydrogen bonds can contribute to the capture of the target. Fig. 5 shows transfer characteristics of the MIP-OFET upon the addition of (*S*)-hyoscyamine. The transfer curves were negatively shifted with the increase of the target alkaloid drug concentration and the corresponding change of the threshold voltages (V_{TH}s) of the OFET provided a sigmoidal titration curve. The negative shift of the transfer curve was derived from the surface potential

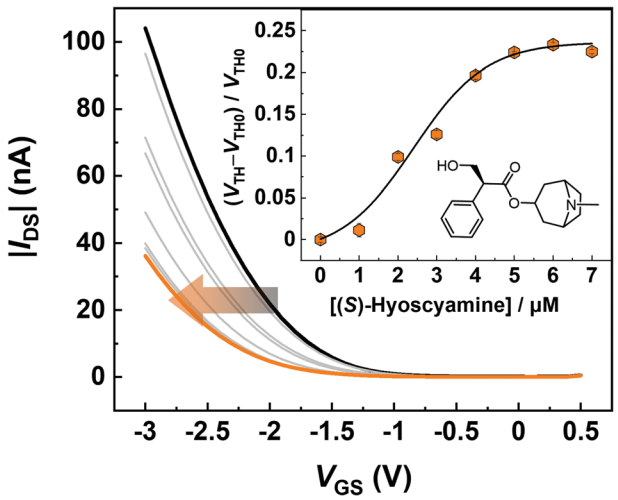

Fig. 5 Transfer characteristics of the MIP-OFET upon the addition of (*S*)-hyoscyamine in a phosphate buffer (100 mM, pH 7.0) containing KCl (100 mM) at 25 °C. Inset represents the titration isotherm corresponding to the (*S*)-hyoscyamine-induced V_{TH} shift. [(*S*)-hyoscyamine] = 0.0–7.0 μM.

change on the extended-gate electrode induced by the accumulation of the positively charged molecules.[19] The sigmoidal response could be due to the hydration of the target.[63] Notably, the OFET-based chemical sensor could achieve highly sensitive detection in contrast to conventional electrochemical apparatuses (*e.g.*, Faraday current response recorded by electrochemical stations)[64] owing to its inherent amplification properties. Indeed, the micromolar level detection implied higher sensitivity in comparison to the conventional electrochemical hyoscyamine sensor.[65]

3.3. Selectivity test

The selectivity of the MIP-OFET was investigated against muscarinic blocking drugs (*i.e.*, (*S*)-hyoscyamine, scopolamine, tropicamide, solifenacin, and oxybutynin),[4] and major metabolites of atropine (*i.e.*, tropic acid and tropine).[66] Fig. 6 represents the highest response to (*S*)-hyoscyamine, stemming from the high complementarity between the target alkaloid and the cavities of the MIP. The components of (*S*)-hyoscyamine, tropine and tropic acid were selected to clarify the contribution skeletons for molecular recognition based on the MIP. The observed moderate response to tropine suggested that the detectability of (*S*)-hyoscyamine by the MIP could rely on the skeleton of 8-azabicyclo[3.2.1]octane over that of 3-hydroxy-2-phenylpropanoate. Remarkably, the MIP succeeded in discriminating (*S*)-hyoscyamine over scopolamine (a close structural analog) because the epoxide moiety on scopolamine would form an intramolecular hydrogen bond with the protonated tertiary amino group (pK_a = 7.8)[67] of scopolamine at pH 7.0. Indeed, DFT calculation (Fig. S14, ESI†) clearly showed the isosurface between the oxygen atom of the epoxide moiety and the protonated tertiary amino group, indicating that the electron density increased owing to the intramolecular hydrogen bond. Such interaction would cause a conformation change and weaken the electrostatic interactions between the

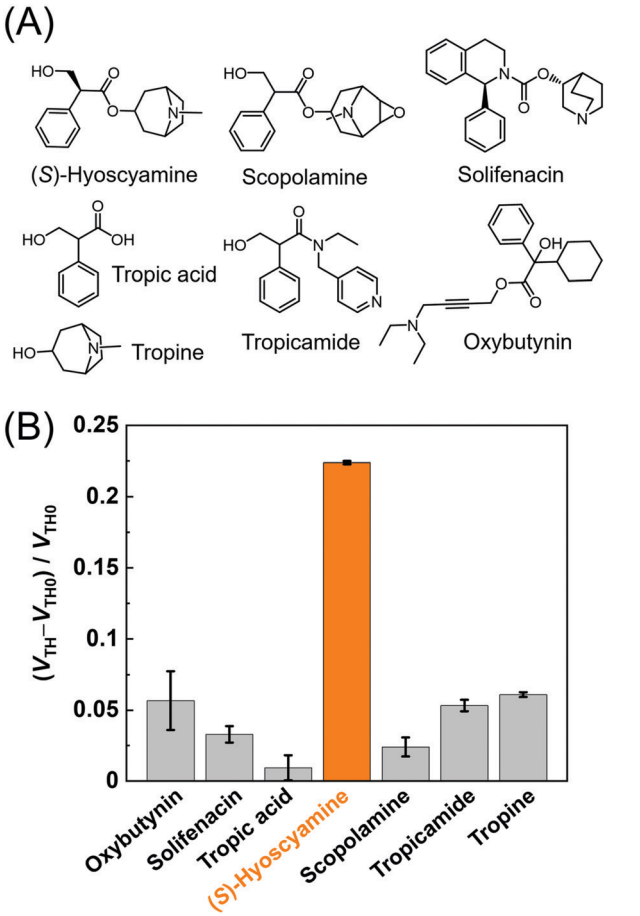

Fig. 6 (A) Chemical structures of muscarinic blocking drugs and metabolites of atropine. (B) Result of the selectivity test against 7 analytes. Three repetitions were carried out for each analyte in a phosphate buffer (100 mM, pH 7.0) containing KCl (100 mM) at 25 °C. [Analyte] = 5.0 μM.

protonated tertiary amino group of scopolamine and the carboxylate group on the MIP, which in turn results in a low affinity for scopolamine.

3.4. Determination of % ee of (*S*)-hyoscyamine

Finally, the % ee determination of (*S*)-hyoscyamine was performed by using the MIP-OFET. Toward the realization of an easy-to-use chemical sensor for OTC drugs,[68] the chiral discriminatory power of the OFET-based sensor[69–71] was evaluated from 0.2 to 90.2% ee according to the enantiomeric purity of the commercially available (*S*)-hyoscyamine (Fig. S15 and S16, ESI†). As shown in Fig. S17 (ESI†), the transistor characteristics shifted by increasing the % ee values of (*S*)-hyoscyamine. In this regard, Fig. 7 shows the linear dependency of the V_{TH} on the % ee of (*S*)-hyoscyamine. Thus, the MIP-OFET seems to have potential as a chemical sensor for OTC drugs in real-world applications.

Conclusions

In summary, we designed and fabricated a chemical sensor based on the MIP-OFET for sensitive and selective discrimination of

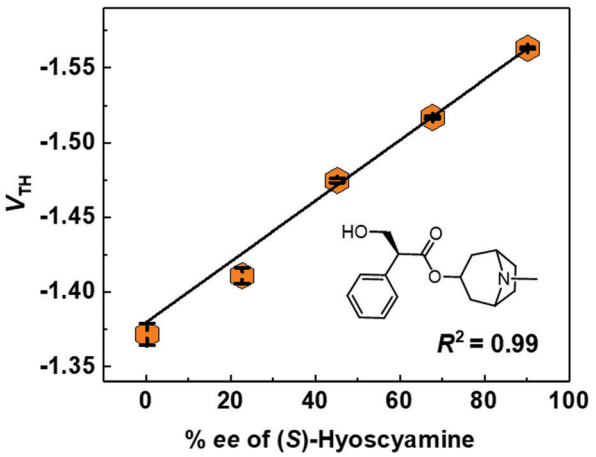

Fig. 7 Threshold voltage (V_{TH}) corresponding to the % ee value of (*S*)-hyoscyamine in a phosphate buffer (100 mM, pH 7.0) containing KCl (100 mM) at 25 °C. The overall hyoscyamine concentration was set to 5.0 μM.

(*S*)-hyoscyamine. DFT calculation was applied for optimizing the ratio design of the MIP components, resulting in an appropriate molar ratio to form the favorable complex of (*S*)-hyoscyamine with monomer units through hydrogen bonds. The MIP-AuNS-attached extended-gate electrode was connected to the OFET and applied to the electrical detection of (*S*)-hyoscyamine. The OFET-based sensor device successfully detected (*S*)-hyoscyamine with high sensitivity. Furthermore, we applied the MIP-OFET to the % ee determination of commercially available (*S*)-hyoscyamine for the evaluation of the usability of the sensor device against OTC drugs in real-world scenarios. We believe that our strategy for the development of analytical devices based on organic electronics could broaden the horizon of the chemical sensing applications in drug analysis.

Author contributions

Q. Z. synthesized and characterized the MIP and NIP and performed the electrochemical measurements; Y. S. and Q. Z. wrote the manuscript; K. O. measured FE-SEM of the MIP and NIP electrodes and operated FT-IR measurements; H. F. and K. O. fabricated the OFET devices and characterized the transistor characteristics; V. M. and C. G. provided helpful discussion; K. H. and T. M. conceived the entire project.

Conflicts of interest

The authors declare no competing financial interest.

Acknowledgements

T. M. gratefully acknowledges the financial support from JSPS KAKENHI (Grant no. JP21H01780, JP20K21204, JP20H05207 and JP22H04524), Core-to-Core Program, ECSJ kanto branch research grant, and JST CREST (Grant no. JPMJCR2011). K. H., C. G. and V. M. acknowledge financial support from the Region Hauts de France and the European Regional Development Fund for co-funding of equipment under CPER 2007–2020. K. H. acknowledges financial support from Institut Universitaire de France. Q. Z. thanks the JSPS, Research Fellow for Young Scientists (DC1) (Grant no. JP22J23433). Y. S. also thanks the JSPS KAKENHI (Grant no. JP22K14706) and the Sasakawa Scientific Research Grant. T. M. also thanks AGC Inc. for supplying CYTOP, TOYOBO Co., Ltd for supplying the PEN film, and Daicel Co., Ltd for the measurements of high-performance liquid chromatography to determine the % ee value of (*S*)-hyoscyamine.

References

1 P. Srinivasan and C. D. Smolke, *Nature*, 2020, **585**, 614–619.
2 J. Schmitz, D. van der Mey, M. Bermudez, J. Klockner, R. Schrage, E. Kostenis, C. Trankle, G. Wolber, K. Mohr and U. Holzgrabe, *J. Med. Chem.*, 2014, **57**, 6739–6750.
3 J. H. Xu, S. C. Zheng, J. W. Zhang, X. Y. Liu and B. Tan, *Angew. Chem., Int. Ed.*, 2016, **55**, 11834–11839.
4 A. M. Lakstygal, T. O. Kolesnikova, S. L. Khatsko, K. N. Zabegalov, A. D. Volgin, K. A. Demin, V. A. Shevyrin, E. A. Wappler-Guzzetta and A. V. Kalueff, *ACS Chem. Neurosci.*, 2019, **10**, 2144–2159.
5 D. J. Meagher, *BMJ*, 2001, **322**, 144–149.
6 M. Hu, H. T. Feng, Y. X. Yuan, Y. S. Zheng and B. Z. Tang, *Coord. Chem. Rev.*, 2020, **416**, 213329.
7 X. L. Chen, Y. Kang and S. Zeng, *Chirality*, 2018, **30**, 609–618.
8 J. Clayden, W. J. Moran, P. J. Edwards and S. R. LaPlante, *Angew. Chem., Int. Ed.*, 2009, **48**, 6398–6401.
9 N. M. Maier, P. Franco and W. Lindner, *J. Chromatogr. A*, 2001, **906**, 3–33.
10 R. Soares, A. K. Singh, E. R. M. Kedor-Hackmann and M. I. R. M. Santoro, *J. AOAC Int.*, 2009, **92**, 1663–1672.
11 D. Castilla-Fernandez, D. Moreno-Gonzalez, J. F. Garcia-Reyes, E. Ballesteros and A. Molina-Diaz, *Food Chem.*, 2021, **347**, 129020.
12 S. Yuvaraja, A. Nawaz, Q. Liu, D. Dubal, S. G. Surya, K. N. Salama and P. Sonar, *Chem. Soc. Rev.*, 2020, **49**, 3423–3460.
13 H. Li, W. Shi, J. Song, H. J. Jang, J. Dailey, J. Yu and H. E. Katz, *Chem. Rev.*, 2019, **119**, 3–35.
14 C. Zhang, P. Chen and W. Hu, *Chem. Soc. Rev.*, 2015, **44**, 2087–2107.
15 L. Torsi, M. Magliulo, K. Manoli and G. Palazzo, *Chem. Soc. Rev.*, 2013, **42**, 8612–8628.
16 C. Liao and F. Yan, *Polym. Rev.*, 2013, **53**, 352–406.
17 M. Y. Mulla, P. Seshadri, L. Torsi, K. Manoli, A. Mallardi, N. Ditaranto, M. V. Santacroce, C. Di Franco, G. Scamarcio and M. Magliulo, *J. Mater. Chem. B*, 2015, **3**, 5049–5057.
18 F. X. Werkmeister, T. Koide and B. A. Nickel, *J. Mater. Chem. B*, 2016, **4**, 162–168.
19 P. Bergveld, *Sens. Actuators, B*, 2003, **88**, 1–20.
20 R. Kubota, Y. Sasaki, T. Minamiki and T. Minami, *ACS Sens.*, 2019, **4**, 2571–2587.
21 Q. Zhou, M. Wang, S. Yagi and T. Minami, *Nanoscale*, 2021, **13**, 100–107.

22 K. Asano, Y. Sasaki, Q. Zhou, R. Mitobe, W. Tang, X. Lyu, M. Kamiko, H. Tanaka, A. Yamagami, K. Hagiya and T. Minami, *J. Mater. Chem. C*, 2021, **9**, 11690–11697.
23 A. K. Yatsimirsky, *Nat. Prod. Commun.*, 2012, **7**, 369–380.
24 M. A. Beatty, A. J. Selinger, Y. Q. Li and F. Hof, *J. Am. Chem. Soc.*, 2019, **141**, 16763–16771.
25 M. Sapotta, A. Hofmann, D. Bialas and F. Wurthner, *Angew. Chem., Int. Ed.*, 2019, **58**, 3516–3520.
26 J. Chen, L. Chen, Y. Zhang, L. Zhao, M. Dong, Z. Meng, Q. Meng and C. Li, *Chem. Commun.*, 2022, **58**, 3370–3373.
27 T. Minami, N. A. Esipenko, B. Zhang, M. E. Kozelkova, L. Isaacs, R. Nishiyabu, Y. Kubo and P. Anzenbacher, Jr., *J. Am. Chem. Soc.*, 2012, **134**, 20021–20024.
28 E. G. Shcherbakova, B. Zhang, S. Gozem, T. Minami, P. Y. Zavalij, M. Pushina, L. D. Isaacs and P. Anzenbacher, Jr., *J. Am. Chem. Soc.*, 2017, **139**, 14954–14960.
29 T. Takeuchi and H. Sunayama, *Chem. Commun.*, 2018, **54**, 6243–6251.
30 L. Chen, X. Wang, W. Lu, X. Wu and J. Li, *Chem. Soc. Rev.*, 2016, **45**, 2137–2211.
31 L. Chen, S. Xu and J. Li, *Chem. Soc. Rev.*, 2011, **40**, 2922–2942.
32 M. J. Whitcombe, I. Chianella, L. Larcombe, S. A. Piletsky, J. Noble, R. Porter and A. Horgan, *Chem. Soc. Rev.*, 2011, **40**, 1547–1571.
33 A. Mier, I. Maffucci, F. Merlier, E. Prost, V. Montagna, G. U. Ruiz-Esparza, J. V. Bonventre, P. K. Dhal, B. T. S. Bui, P. Sakhaii and K. Haupt, *Angew. Chem., Int. Ed.*, 2021, **60**, 20849–20857.
34 E. Paruli, T. Griesser, F. Merlier, C. Gonzato and K. Haupt, *Polym. Chem.*, 2019, **10**, 4732–4739.
35 Y. H. Shim, E. Yilmaz, S. Lavielle and K. Haupt, *Analyst*, 2004, **129**, 1211–1215.
36 J. Zuo, X. Zhang, X. Li, Z. Li, Z. Li, H. Li and W. Zhang, *RSC Adv.*, 2019, **9**, 19712–19719.
37 M. P. Chantada-Vazquez, J. Sanchez-Gonzalez, E. Pena-Vazquez, M. J. Tabernero, A. M. Bermejo, P. Bermejo-Barrera and A. Moreda-Pineiro, *Biosens. Bioelectron.*, 2016, **75**, 213–221.
38 P. Lenain, J. D. Di Mavungu, P. Dubruel, J. Robbens and S. De Saeger, *Anal. Chem.*, 2012, **84**, 10411–10418.
39 J. Sun, L. Zhang, X. Liu, A. Zhao, C. Hu, T. Gan and Y. Liu, *J. Electroanal. Chem.*, 2021, **903**, 115843.
40 A. Khataee, J. Hassanzadeh and E. Kohan, *Spectrochim. Acta, Part A*, 2018, **205**, 614–621.
41 J. Abbasifar and A. Samadi-Maybodi, *J. Fluoresc.*, 2016, **26**, 1645–1652.
42 M. Nakamura, M. Ono, T. Nakajima, Y. Ito, T. Aketo and J. Haginaka, *J. Pharm. Biomed. Anal.*, 2005, **37**, 231–237.
43 Y. B. Wei, Q. Zeng, J. Z. Huang, X. R. Guo, L. L. Wang and L. S. Wang, *ACS Appl. Mater. Interfaces*, 2020, **12**, 24363–24369.
44 A. Wojnarowicz, P. S. Sharma, M. Sosnowska, W. Lisowski, T. P. Huynh, M. Pszona, P. Borowicz, F. D'Souza and W. Kutner, *J. Mater. Chem. B*, 2016, **4**, 1156–1165.
45 H. da Silva, J. G. Pacheco, J. Magalhaes, S. Viswanathan and C. Delerue-Matos, *Biosens. Bioelectron.*, 2014, **52**, 56–61.
46 N. Leibl, L. Duma, C. Gonzato and K. Haupt, *Bioelectrochemistry*, 2020, **135**, 107541.
47 Z. Iskierko, A. Checinska, P. S. Sharma, K. Golebiewska, K. Noworyta, P. Borowicz, K. Fronc, V. Bandi, F. D'Souza and W. Kutner, *J. Mater. Chem. C*, 2017, **5**, 969–977.
48 T. Kajisa, W. Li, T. Michinobu and T. Sakata, *Biosens. Bioelectron.*, 2018, **117**, 810–817.
49 Z. Iskierko, P. S. Sharma, K. R. Noworyta, P. Borowicz, M. Cieplak, W. Kutner and A. M. Bossi, *Anal. Chem.*, 2019, **91**, 4537–4543.
50 S. Beyazit, B. T. S. Bui, K. Haupt and C. Gonzato, *Prog. Polym. Sci.*, 2016, **62**, 1–21.
51 I. McCulloch, M. Heeney, C. Bailey, K. Genevicius, I. Macdonald, M. Shkunov, D. Sparrowe, S. Tierney, R. Wagner, W. Zhang, M. L. Chabinyc, R. J. Kline, M. D. McGehee and M. F. Toney, *Nat. Mater.*, 2006, **5**, 328–333.
52 M. J. Frisch, G. W. Trucks, H. B. Schlegel, G. E. Scuseria, M. A. Robb, J. R. Cheeseman, G. Scalmani, V. Barone, G. A. Petersson, H. Nakatsuji, X. Li, M. Caricato, A. V. Marenich, J. Bloino, B. G. Janesko, R. Gomperts, B. Mennucci, H. P. Hratchian, J. V. Ortiz, A. F. Izmaylov, J. L. Sonnenberg, D. Williams-Young, F. Ding, F. Lipparini, F. Egidi, J. Goings, B. Peng, A. Petrone, T. Henderson, D. Ranasinghe, V. G. Zakrzewski, J. Gao, N. Rega, G. Zheng, W. Liang, M. Hada, M. Ehara, K. Toyota, R. Fukuda, J. Hasegawa, M. Ishida, T. Nakajima, Y. Honda, O. Kitao, H. Nakai, T. Vreven, K. Throssell, J. A. Montgomery Jr., J. E. Peralta, F. Ogliaro, M. J. Bearpark, J. J. Heyd, E. N. Brothers, K. N. Kudin, V. N. Staroverov, T. A. Keith, R. Kobayashi, J. Normand, K. Raghavachari, A. P. Rendell, J. C. Burant, S. S. Iyengar, J. Tomasi, M. Cossi, J. M. Millam, M. Klene, C. Adamo, R. Cammi, J. W. Ochterski, R. L. Martin, K. Morokuma, O. Farkas, J. B. Foresman and D. J. Fox, *Gaussian 16 (Revision C.01)*, Gaussian, Inc., Wallingford CT, 2016.
53 X. Feása, C. A. Fente, S. V. Hosseini, J. A. Seijas, B. I. Vázquez, C. M. Franco and A. Cepeda, *Mater. Sci. Eng., C*, 2009, **29**, 398–404.
54 G. Pan, Q. Guo, Y. Ma, H. Yang and B. Li, *Angew. Chem., Int. Ed.*, 2013, **52**, 6907–6911.
55 R. Krishnan, J. S. Binkley, R. Seeger and J. A. Pople, *J. Chem. Phys.*, 1980, **72**, 650–654.
56 G. W. Spitznagel, T. Clark, P. V. Schleyer and W. J. Hehre, *J. Comput. Chem.*, 1987, **8**, 1109–1116.
57 P. J. Stephens, F. J. Devlin, C. F. Chabalowski and M. J. Frisch, *J. Phys. Chem.*, 1994, **98**, 11623–11627.
58 S. Grimme, J. Antony, S. Ehrlich and H. Krieg, *J. Chem. Phys.*, 2010, **132**, 154104.
59 R. Dennington, T. A. Keith and J. M. Millam, *Gaussview (version 6.0.16)*, Semichem Inc., Wallingford, CT, 2016.
60 Y. Liu, Z. Liu, F. Zhao and Y. Tian, *Angew. Chem., Int. Ed.*, 2021, **60**, 14429–14437.
61 S. Motia, B. Bouchikhi, E. Llobet and N. El Bari, *Talanta*, 2020, **216**, 120953.
62 U. Domanska, A. Pobudkowska, A. Pelczarska and P. Gierycz, *J. Phys. Chem. B*, 2009, **113**, 8941–8947.
63 Z. Mskolczy, M. Megyesi, O. Toke and L. Biczok, *Phys. Chem. Chem. Phys.*, 2019, **21**, 4912–4919.

64 F. Yan, M. Zhang and J. Li, *Adv. Healthcare Mater.*, 2014, **3**, 313–331.
65 S. S. Badawy, Y. M. Issa and A. A. Mutair, *J. Pharm. Biomed. Anal.*, 2005, **39**, 117–124.
66 M. J. Vandermeer, H. K. L. Hundt and F. O. Muller, *J. Pharm. Pharmacol.*, 1986, **38**, 781–784.
67 H. Weinstein, S. Srebrenik, S. Maayani and M. Sokolovsky, *J. Theor. Biol.*, 1977, **64**, 295–309.
68 Y. Sasaki, S. Kojima, V. Hamedpour, R. Kubota, S. Y. Takizawa, I. Yoshikawa, H. Houjou, Y. Kubo and T. Minami, *Chem. Sci.*, 2020, **11**, 3790–3796.
69 M. Y. Mulla, E. Tuccori, M. Magliulo, G. Lattanzi, G. Palazzo, K. Persaud and L. Torsi, *Nat. Commun.*, 2015, **6**, 6010.
70 Y. Sun, Y. Wang, Y. Wu, X. Wang, X. Li, S. Wang and Y. Xiao, *Anal. Chem.*, 2018, **90**, 9264–9271.
71 X. Wang, Y. Wang, Y. Wu and Y. Xiao, *Analyst*, 2019, **144**, 2611–2617.